

Free Lunch for Co-Saliency Detection: Context Adjustment

Lingdong Kong¹ Prakhar Ganesh², Tan Wang¹, Junhao Liu³, Yao Chen², Le Zhang⁴

¹Nanyang Technological University, Singapore ²Advanced Digital Sciences Center, University of Illinois at Singapore

³Shenzhen Institute of Advanced Technology, Chinese Academy of Sciences

⁴Institute for Infocomm Research, Agency for Science, Technology and Research (A*STAR)

{lingdong001,tan317}@e.ntu.edu.sg, {prakhar.g,yao.chen}@adsc-create.edu.sg,
jh.liu@siat.ac.cn, zhangleuestc@gmail.com

Abstract

We unveil a long-standing problem in the prevailing co-saliency detection systems: there is indeed inconsistency between training and testing. Constructing a high-quality co-saliency detection dataset involves time-consuming and labor-intensive pixel-level labeling, which has forced most recent works to rely instead on semantic segmentation or saliency detection datasets for training. However, the lack of proper co-saliency and the absence of multiple foreground objects in these datasets can lead to spurious variations and inherent biases learned by models. To tackle this, we introduce the idea of counterfactual training through context adjustment, and propose a “cost-free” group-cut-paste (GCP) procedure to leverage images from off-the-shelf saliency detection datasets and synthesize new samples. Following GCP, we collect a novel dataset called Context Adjustment Training. The two variants of our dataset, i.e., CAT and CAT+, consist of 16,750 and 33,500 images, respectively. All images are automatically annotated with high-quality masks. As a side-product, object categories, as well as edge information, are also provided to facilitate other related works. Extensive experiments with state-of-the-art models are conducted to demonstrate the superiority of our dataset. We hope that the scale, diversity, and quality of CAT/CAT+ can benefit researchers in this area and beyond. The dataset and benchmark toolkit will be accessible through our project page.

1. Introduction

Saliency detection attempts to mimic the human visual system by automatically detecting and segmenting out object regions that attract the most attention in an image [3]. Today’s saliency detection systems, especially those equipped with deep neural networks [55], are good at identifying salient objects from images [3]. However, the set-

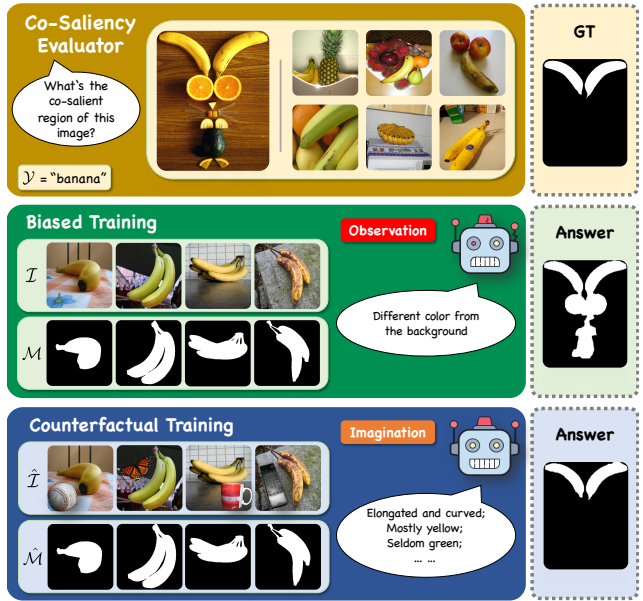


Figure 1. Conceptual illustration of counterfactual training versus biased training. **Top block:** Evaluation for the *banana* group in *CoSOD3k* dataset [19]; **Middle block:** Biased training samples from current co-saliency detection datasets; **Bottom block:** Samples generated under the idea of counterfactual training. **GT** denotes the ground-truth. **Answers** are generated by *GICD* [66].

ting of detecting a single object is ideal. For real-world applications like image/video retrieval [28], surveillance [22], video analysis [27], etc., there are always scenes that multiple objects co-occurring in or across frames. This motivates our community to explore co-saliency detection [26]. Sharing a similar rationale with saliency detection, co-saliency detection automatically detects and segments out the common object regions that attract the most attention within image groups [55]. Such an imitation can be achieved by the learning paradigm hiding behind artificial neural networks, especially convolutional neural networks [33]. However,

“there is no such thing as a free lunch.” The success of deep learning systems depends heavily on large-scale datasets, which take huge effort and time to collect. The conventional way [19, 66] of constructing a specialized co-saliency detection dataset involves time-consuming and labor-intensive data selection and pixel-level labeling. As shown in Figure 1, the uni-object distribution of the current training data (middle block) has deviated heavily from that of the evaluation data (top block), which consists of complex context with multiple foreground objects. Models encoded with such spurious variations and biases fail to capture the co-salient signals and thus make incorrect predictions [51, 25].

In the context of co-saliency detection, we denote the training, testing, and true (real-world) distributions as \mathcal{D} , \mathcal{E} , and \mathcal{T} , respectively. Recent works on evaluation [19, 66] make \mathcal{E} one-step closer towards \mathcal{T} by identifying co-salient signals from multi-foreground clusters in a group-by-group manner. However, a dataset that can well-define \mathcal{D} is still missing. As we will discuss in Section 2, most recent works borrow semantic segmentation datasets like *MS-COCO* [38] and saliency detection datasets like *DUTS* [53] to train their models, which exacerbate the inconsistency among \mathcal{D} , \mathcal{E} , and \mathcal{T} . Not surprisingly, as models only see naive examples during training, they will inevitably cater to the seen idiosyncrasies, and thus are stuck in the unseen world with biased assumptions.

In this paper, we aim at finding a “cost-free” way to handle the distribution inconsistency in co-saliency detection. Intrigued by causal effect [46, 45] and its extensions in vision & language [54, 42, 60], we introduce **counterfactual training** with regard to the gap between current training distribution \mathcal{D} and true distribution \mathcal{T} as the direct cause [44, 50] of incorrect co-saliency predictions. As shown in Figure 2, the quality of prediction \mathcal{P} made by a learning-based model is dependent on the quality of input data \mathcal{I} under distribution \mathcal{D} . The goal of counterfactual training is to synthesize “imaginary” data sample $\hat{\mathcal{I}}$, whose distribution $\hat{\mathcal{D}}$ — also originates from \mathcal{D} — can mimic \mathcal{T} . In this way, models can capture the true effect in terms of co-saliency from $\hat{\mathcal{I}}$ and make prediction $\hat{\mathcal{P}}$ properly.

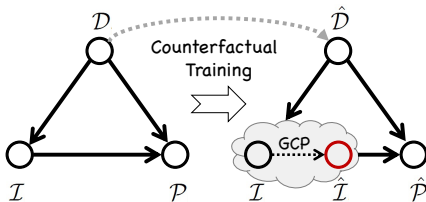


Figure 2. Causal graph for co-saliency detection. Nodes denote variables and arrows denote direct causal effects.

Under the instruction of counterfactual training, we propose using context adjustment [13] to augment off-the-shelf saliency detection datasets, and introduce a novel **group-cut-paste (GCP)** procedure to improve the distribution of the training dataset. Taking a closer look at Figure 1, \mathcal{M} and \mathcal{Y} are the corresponding pixel-level annotation and cat-

egory label of sample \mathcal{I} . GCP turns \mathcal{I} into a canvas to be completed and paint the remaining part through the following steps: (1) classifying candidate images into a semantic group \mathcal{Z} (e.g., *banana*) by reliable pretrained models; (2) cutting out candidate objects (e.g., *baseball*, *butterfly*, etc.); and (3) pasting candidate objects into image samples. We will revisit this procedure formally in Section 3. Different from the plain “observation” (e.g., *different color from the background*) made by biased training, counterfactual training opens the door of “imagination” and allows models to think comprehensively [42]. A better prediction can be made possibly because of features, such as the “*elongated and curved*” shape (instead of the *round* shape of *baseball* and *orange*) or “*yellow-green*” color (instead of the *dark* color of *remote control* and *avocado*), are captured. In this way, models can focus more on the true causal effects rather than spurious variants and biases caused by the distribution gap [5].

Following GCP, we collect a novel dataset called **Context Adjustment Training**, of which has two variants: **CAT** and **CAT+**. Both of them consist of 280 subclasses affiliated to 15 superclasses, which cover common items in daily life, as well as animals and plants in nature. While our CAT/CAT+ is diverse in semantics, it also has a large scale. The two variants of our dataset contain 16,750 and 33,500 samples, respectively, making it the current largest in co-saliency detection. Every sample in CAT/CAT+ is equipped with sophisticated mask annotation, category, and edge information. It is worth noting that, unlike manual selection and pixel-by-pixel labeling, all the images and their corresponding masks in our dataset are automatically annotated, making the cost virtually “free.” Extensive experimental results shown in Section 4 verify the effectiveness of our dataset. Without bells and whistles, CAT/CAT+ helps both one-stage and two-stage models to achieve significant improvements for 5% ~ 30% in conventionally-adopted metrics on challenging evaluation datasets *CoSOD3k* [19] and *CoCA* [66].

2. Related Work

Context Adjustment. Modeling visual contexts liberates a lot of computer vision tasks from the impediment caused by the need for sophisticated annotations [14], such as bounding boxes and pixel-level masks. [61] leverages training pixels and regularization effects of regional dropout by cutting and pasting image patches. To avoid overfitting, [12] randomly masks out square regions of an image during training. The generic vicinal distribution introduced in [63] helps to synthesize the groundtruth of new samples by the linear interpolation of one-hot labels. Unfortunately, the patches introduced by both [61] and [12] may cause severe occlusions for original objects, which is not compatible with the idea of saliency detection [15]. For [63], the

#	Training Dataset	Year	#Img.	#Cat.	#Avg.	#Max.	#Min.	Mul.	Sal.	Larg.	H.Q.	Type	Inputs
1	MSRCv1 [56]	2005	240	8	30.0	30	30	✗	✓	✗	✗	CO	Group images
2	MSRCv2 [56]	2005	591	23	25.7	34	21	✗	✓	✗	✗	CO	Group images
3	iCoseg [2]	2010	643	38	16.9	41	4	✗	✓	✗	✓	CO	Group images
4	MSRA-B [29]	2013	5,000	-	-	-	-	✗	✓	✗	✓	SD	Single image
5	Coseg-Rep [10]	2013	572	23	24.8	116	9	✗	✓	✗	✓	CO	Group images
6	DUT-OMRON [57]	2013	5,172	-	-	-	-	✗	✓	✗	✓	SD	Single image
7	THUR-15K [6]	2014	15,531	5	3,000.0	3,457	2,892	✗	✓	✓	✓	CO	Group images
8	MSRA10K [7]	2015	10,000	-	-	-	-	✗	✓	✓	✓	SD	Single image
9	CoSal2015 [62]	2015	2,015	50	40.3	52	26	✓	✓	✗	✓	CO	Group images
10	DUTS-TR [53]	2017	10,553	-	-	-	-	✗	✓	✓	✓	SD	Single image
11	COCO9213 [38]	2017	9,213	65	141.7	468	18	✓	✓	✗	✗	SS	Group images
12	COCO-GWD [34]	2019	9,000	118	76.2	-	-	✓	✓	✗	✗	SS	Group images
13	COCO-SEG [52]	2019	200,932	78	2576.1	49,355	201	✓	✗	✓	✗	SS	Group images
14	WISD [59]	2019	2,019	-	-	-	-	✓	-	✗	-	CO	Single image
15	DUTS-Class [66]	2020	8,250	291	28.3	252	5	✗	✓	✓	✓	CO	Group images
16	Jigsaw [66]	2020	33,000	291	113.4	1,008	20	✓	✗	✓	✓	CO	Group images
17	CAT (Ours)	2021	16,750	280	59.8	412	14	✓	✓	✓	✓	CO	Group images
18	CAT+ (Ours)	2021	33,500	280	119.6	824	28	✓	✓	✓	✓	CO	Group images

Table 1. Datasets used for training co-saliency detection models. **#Img.**: Number of images; **#Cat.**: Number of categories; **#Avg.**: Average number of images per category; **#Max.**: Maximum number of images per group; **#Min.**: Minimum number of images per group. **Mul.**: Whether contains multiple foreground objects or not; **Sal.**: Whether maintains saliency or not; **Larg.**: Whether large-scale (more than 10k images) or not; **H.Q.**: Whether has high-quality annotations or not. **CO**: Co-saliency detection dataset; **SD**: Saliency detection dataset; **SS**: Semantic segmentation dataset. “-” denotes “not available”.

local statistics and semantic are destroyed. Since the foreground and background are blended, the saliency cannot be appropriately defined anymore. [24] fixes this problem by mixing several transformed versions of an image together, i.e., augmentation chain. Although such a composition improves the model robustness, it cannot introduce co-salient signals. [66] concatenates two samples together to form a multi-foreground image. However, for backbones that require fixed-size inputs [48], the resize of such jigsawed images leads to severe shape distortion. In contrast, our GCP preserves both the multi-foreground requirement and object shapes and maintains saliency [15].

Co-Saliency Detection. The origin of this task can be dated back to the last decade [26], where co-saliency was defined as the regions of an object which occur in a pair of images [36]. A more formal definition given in [35] exploits both intra-image saliency and inter-image saliency in a group-by-group manner. Since then, researchers in this area have been working on identifying co-salient signals across image groups [6]. Representative works from early years [4, 20, 40] rely on certain heuristics like background prior [58] and color contrast [9]. Let alone the post-processing like CRF [32], most modern co-saliency detection models can be divided into two-stage and one-stage models. Building upon saliency detection frameworks, two-stage models leverage the intra-saliency with inter-saliency generated by specially designed modules [30, 18]. There are also some one-stage models which do not require saliency preparation. [65] and [66] introduce consensus embedding procedures to explore group representation and use it to guide soft attentions [68]. Some recent models adopt different network structures to identify co-salient signals, such as graph neural networks [64, 37] and generative adversarial networks [47].

Associating with our dataset, both two-stage and one-stage models achieve better performances.

Training Dataset. Due to the lack of a suitable training dataset, most previous works use existing saliency detection datasets or semantic segmentation datasets for training. Table 1 summarizes datasets adopted to train co-saliency detection models. Small datasets [56, 2, 10] are popular among works in early years only. Some large-scale saliency detection datasets [57, 7, 53] are adopted by two-stage models to extract intra-saliency cues. However, such datasets do not have class information, hence it is impossible for them to train end-to-end models. Some works even borrow datasets from semantic segmentation, e.g., *COCO-SEG* [52] and *COCO9213* [38]. Unfortunately, although such datasets are large in scales, their annotations are coarse. Recently, *DUTS-Class* [66] and its jigsawed version [66] have been proposed as a “transition plan” towards co-saliency. However, the former is just a “grouped” saliency detection dataset, while the latter introduces issues like shape distortion and independent boundaries. Evidence shows that these inappropriate training paradigms have caused serious biases for co-saliency detection models [19, 66]. Our dataset addresses the aforementioned problems. CAT/CAT+ is currently the largest co-saliency detection dataset and offers diverse semantics and high-quality annotations.

Evaluation Dataset. Pioneer co-saliency detection works evaluate model performances on small datasets like *MSRC* [56], *iCoseg* [2], and *ImagePair* [36]. Consisting of 2,015 images from 50 groups, *CoSal2015* [62] is the most popular choice among modern models. However, most samples in it are still uni-object. Two recent datasets [19, 66] fill the defect in terms of both scale and appearance. *CoSOD3k* [19] is a diverse dataset consists of 160 categories and 3,316

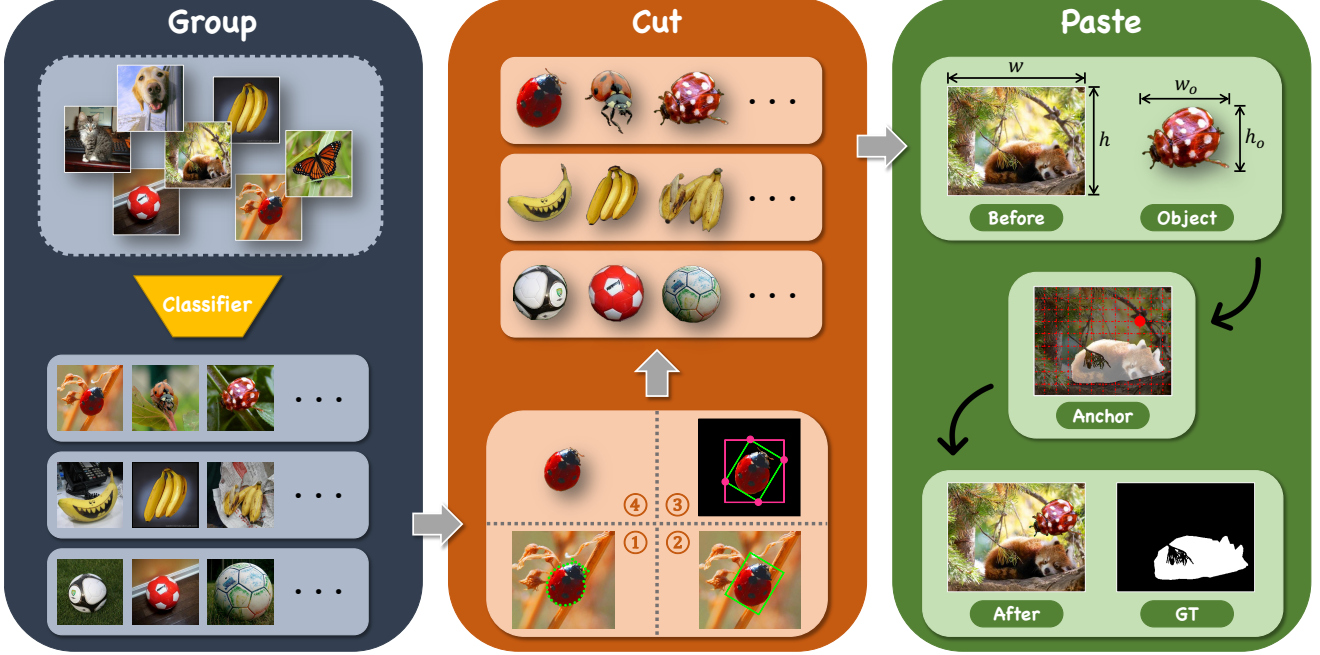


Figure 3. Overview of our group-cut-paste (GCP) procedure. **Left block:** Classifier $\mathcal{F}(\cdot)$ generates category label \mathcal{Y} for all raw images and “group” them accordingly; **Middle block:** Object o is “cut” out from the original image based on contours $\{(p, q)_n\}$ and bounding boxes; **Right block:** New sample $\hat{\mathcal{I}}$ is synthesized by “pasting” randomly sampled object o into canvas \mathcal{I} .

images. 70% and 20% images have one and two objects, while 10% images have three or more objects. CoCA [66] consists of 80 categories with 1,295 images, which are challenging in occlusion and clutter background. At least one foreground object is introduced for every image, and some of them have more than two co-salient objects. We have adopted both of these two datasets to evaluate model performances in our benchmark experiments.

3. Proposed Method

In this section, we first introduce the idea of counterfactual training in co-saliency detection. Under this high-level instruction, we propose a group-cut-paste (GCP) procedure to adjust visual context and generate training samples. Finally, we construct a novel dataset by following GCP.

3.1. Counterfactual Training

Let $\mathcal{I} \in \mathbb{R}^{w \times h \times c}$ and $\mathcal{M} \in \mathbb{R}^{w \times h}$ denote a training image and its mask annotation with width w , height h , and channel c . \mathcal{Z} is an image group whose members include \mathcal{I} . \mathcal{Y} denotes the category label which contains the semantic information for both \mathcal{Z} and \mathcal{I} . The counterfactual [43] $\hat{\mathcal{I}} = \mathcal{I}_{\mathcal{M}}[\hat{\mathcal{Z}}(\hat{\mathcal{I}})]$ of sample \mathcal{I} , is read as:

\mathcal{I} would be $\hat{\mathcal{I}}$, had \mathcal{M} been $\hat{\mathcal{M}}$,
given the fact that $\mathcal{Z} = \hat{\mathcal{Z}}(\mathcal{I} = \hat{\mathcal{I}})$.

where $\hat{\mathcal{Z}} \supset \hat{\mathcal{I}}$ denotes the new image group; New mask is restricted as $\hat{\mathcal{M}} \approx \mathcal{M}$ to maintain the saliency [15] of the co-occurring object. In other words, label \mathcal{Y} will not change during the whole process. The given “fact” $\mathcal{Z} = \hat{\mathcal{Z}}(\hat{\mathcal{I}})$ means that the group training paradigm remains the same, while the “counter-fact” (what if) $\mathcal{M} \neq \hat{\mathcal{M}}(\hat{\mathcal{I}})$ is indicating that the generated $\hat{\mathcal{M}}(\hat{\mathcal{I}})$ clashes with $\hat{\mathcal{M}}$.

The conceptual meanings of counterfactual training can be substantiated by the following instructions [45]:

Abduction - “Given the fact that $\mathcal{Z} = \hat{\mathcal{Z}}(\mathcal{I} = \hat{\mathcal{I}})$.” When constructing a new image group $\hat{\mathcal{Z}}$ for \mathcal{Z} , the co-saliency should remain unchanged. That is to say, the “fact” that the object in $\mathcal{I} \subset \mathcal{Z}$ is salient still holds for it in $\hat{\mathcal{I}} \subset \hat{\mathcal{Z}}$.

Action - “Had \mathcal{M} been $\hat{\mathcal{M}}$.” After the “imagination”, the mask annotation $\hat{\mathcal{M}}$ should not have a significant change. Here we intervene \mathcal{M} by keeping the semantic label \mathcal{Y} the same both beforehand and afterward.

Prediction - “ \mathcal{I} would be $\hat{\mathcal{I}}$.” Conditioning on the “fact” $\mathcal{Z} = \hat{\mathcal{Z}}(\hat{\mathcal{I}})$ and the intervention objective $\mathcal{M} \approx \hat{\mathcal{M}}$, we can generate the counterfactual sample $\hat{\mathcal{I}}$ and its mask $\hat{\mathcal{M}}$ from the following probability distribution function: $P(\mathcal{I} | \mathcal{Z} = \hat{\mathcal{Z}}(\hat{\mathcal{I}}), \mathcal{M} \approx \hat{\mathcal{M}})$.

3.2. Group-Cut-Paste

Following the counterfactual training instructions, we design this group-cut-paste (GCP) procedure. Specifically, the object map $\mathcal{O} \in \mathbb{R}^{w \times h \times c}$ for image \mathcal{I} can be generated by \mathcal{M} , i.e., $\mathcal{O} = \mathcal{I} \odot \mathcal{M}$, where \odot denote element-wise mul-

tiplication. The goal of GCP is to automatically generate a new training sample $(\hat{\mathcal{I}}, \hat{\mathcal{M}})$ by combining \mathcal{I}_a and \mathcal{M}_a with \mathcal{O}_b , where a and b are category indexes of the target and source groups, respectively. The generated sample $(\hat{\mathcal{I}}, \hat{\mathcal{M}})$ is then used to train candidate models with their original loss functions. Figure 3 gives an overview of our method.

Group. The first step is to build image groups. To effectively classify candidate images, we adopt one of the current state-of-the-art classifiers *WSL-Images* [41], which achieves 85.4% Top-1 accuracy on *ImageNet* [11]. The category label \mathcal{Y} can be generated by $\mathcal{Y} = \mathcal{F}(\mathcal{I})$, where $\mathcal{F}(\cdot)$ denotes the pretrained classifier. We manually pick out the misclassified examples after grouping. This results in $\{(\mathcal{I}, \mathcal{Y}), \mathcal{M}\}$ sample pairs distributed in z semantic groups.

Cut. Both object map \mathcal{O} and mask \mathcal{M} are used to prepare candidate object o . We adopt the *border following algorithm* [49] to extract n external contour points $\{(p, q)_n\}$ by mask \mathcal{M} . Based on contours, the bounding rectangle with minimum area can be drawn. The area to be cut can then be defined by the four vertices of this rotated box. This gives us the final object $o \in \mathbb{R}^{w_o \times h_o \times c}$.

Paste. Under the counterfactual training instructions, object o can be pasted properly into \mathcal{I} to form a new sample $\hat{\mathcal{I}}$. Here we maintain the “fact” by preserving group consistency, i.e., conduct this procedure in a group-by-group manner. Denote the regions outside \mathcal{M} as $\bar{\mathcal{M}}$. To avoid severe occlusion, coordinate (x, y) is randomly sampled in $\bar{\mathcal{M}}$ as the position to be pasted. The center of o is chosen as the anchor for pasting. We execute the “action” by restricting the size of candidate object o and maintaining label \mathcal{Y} before and after paste. The mask annotations $\hat{\mathcal{M}}$ are automatically synthesized by dyadic operations between o and \mathcal{M} . Finally, under uniform probability distribution $P = 1/(z-1)$, “prediction” gives us $\{(\hat{\mathcal{I}}, \mathcal{Y}), \hat{\mathcal{M}}\}$ pairs for further model training. Our GCP operation can be easily applied on CPUs in parallel with the main GPU training tasks, which hides the computation cost and boosts the performance for virtually free.

3.3. Constructing the Dataset

For the purpose of stabilization and to ensure high quality, we collect a dataset called Context Adjustment Training. We pick 8,375 images with clear saliency and sophisticated annotations as our canvas from existing saliency detection datasets [53, 15]. Following GCP, 280 semantic groups affiliated to 15 superclasses are built after the “grouping,” i.e., aves, electronic product (elec.), food, fruit, insect, instrument (instru.), kitchenware (kitch.), mammal (mamm.), marine, other, reptile (rept.), sports, tool, transportation (trans.), and vegetable (vege.). See Figure 4 for the taxonomy. We then “cut” all the objects o out and discard those with incomplete shapes. During the “paste” stage, the object size is restricted as $\frac{w_o}{w} = \frac{h_o}{h} = (0.1 \sim 0.3)$.

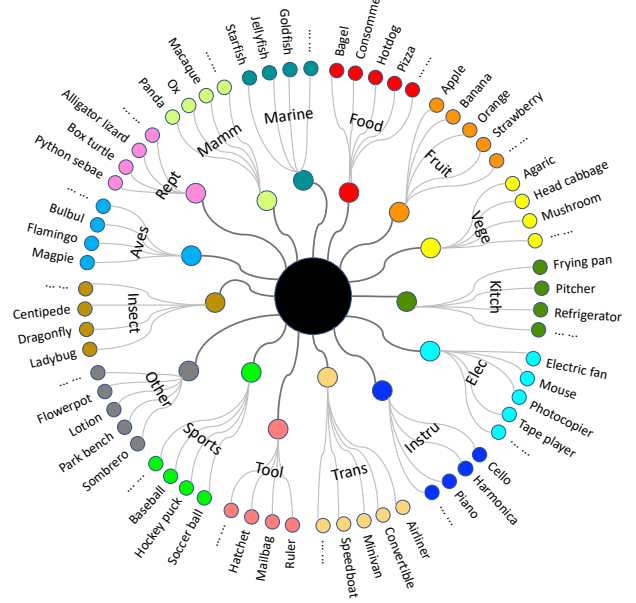


Figure 4. The taxonomic illustration for our dataset, of which consists of 15 superclasses and 280 subclasses. Zoom in for details.

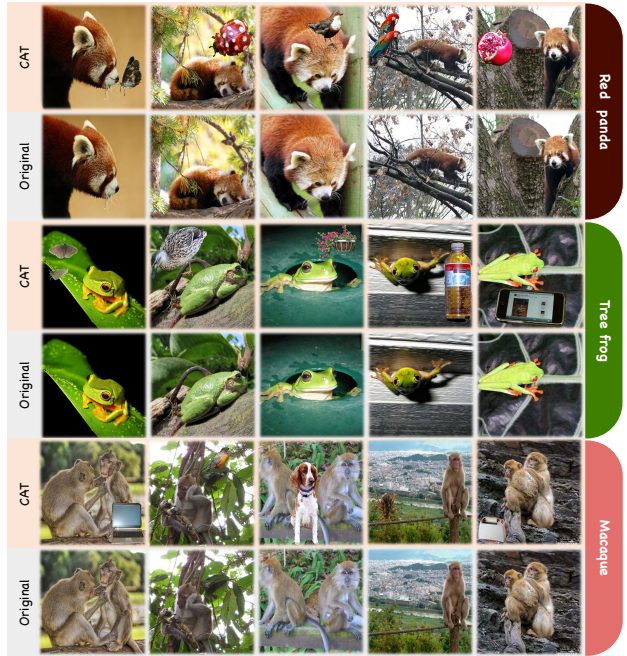


Figure 5. Samples from our dataset. Zoom in for details.

Candidate objects are randomly flipped horizontally to increase diversity. We sample twice for each candidate image to generate two samples and do a re-sample for unsatisfied cases. This gives us 16,750 augmented images. Their corresponding masks are automatically generated. As shown in Figure 5, samples synthesized by counterfactual training and GCP can model realistic visual context and offer proper co-salient signals.

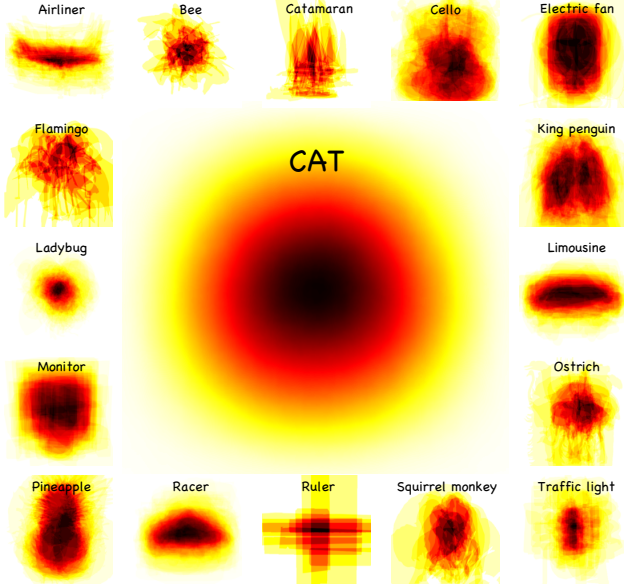


Figure 6. Patterns for representative groups and the overall dataset. Best viewed in color and zoomed-in for details.

Our dataset has two variants: CAT and CAT+. CAT consists of all 16,750 augmented images, while CAT+ contains both the augmented and two times of the original images (i.e., 33,500 images, which is ten times bigger than the current largest evaluation dataset). In short, CAT+ is larger in scale, and CAT is more challenging in terms of the quota of complex contexts. See Table 1 for more dataset statistics. Some patterns (calculated by averaging overlapping masks) of our dataset are shown in Figure 6. The overall pattern of our dataset tends to be a “round” shape, while categories with unique shapes (e.g., *cello* and *limousine*) result in shape-biased patterns, which is consistent with the definition of saliency [15]. More details of our dataset can be found in [supplementary material](#).

4. Benchmark Experiment

In this section, we conduct a comprehensive benchmark study for co-saliency detection to verify the effectiveness and superiority of our proposed methods and dataset.

4.1. Implementation Detail

Training. We compare our CAT/CAT+ with five popular datasets, i.e., *COCO-SEG* [52], *DUTS-TR* [53], *COCO9213* [38], *DUTS-Class* [66], and *Jigsaw* [66]. Four current state-of-the-art models are selected for our benchmark experiments, i.e., *PoolNet* [39], *EGNet* [67], *ICNet* [30], and *GICD* [66]. During training, all input data, including images, masks, and edges maps, are resized to 224×224 before feeding into the networks. NVIDIA GeForce RTX 2080Ti graphics cards are used through our experiments. **Models.** For *PoolNet* [39], we adopt its Res2Net [21] ver-

CoSOD3k [19]	MAE ↓	F_{max} ↑	F_{avg} ↑	E_{max} ↑	E_{avg} ↑	S_{α} ↑
DUTS-TR [‡] [53]	0.2089	0.5177	0.4710	0.7249	0.6463	0.6205
DUTS-Class [66]	0.2049	0.5077	0.4703	0.7102	0.6495	0.5906
Jigsaw [66]	0.1895	0.5437	0.5029	0.7415	0.6770	0.6195
COCO9213 [38]	0.2255	0.4883	0.4525	0.7195	0.6390	0.6012
CAT (Ours)	0.1760	0.5503	0.5089	0.7424	0.6783	0.6288
CAT+ (Ours)	0.1713	0.5614	0.5281	0.7509	0.6886	0.6355

CoCA [66]	MAE ↓	F_{max} ↑	F_{avg} ↑	E_{max} ↑	E_{avg} ↑	S_{α} ↑
DUTS-TR [‡] [53]	0.2350	0.2993	0.2732	0.6764	0.5582	0.5254
DUTS-Class [66]	0.2102	0.3230	0.2987	0.6953	0.5945	0.5347
Jigsaw [66]	0.2224	0.3238	0.2941	0.7008	0.5705	0.5470
COCO9213 [38]	0.2558	0.2833	0.2613	0.6975	0.5413	0.5095
CAT (Ours)	0.1820	0.3348	0.3070	0.7075	0.6207	0.5555
CAT+ (Ours)	0.1809	0.3459	0.3230	0.7071	0.6253	0.5605

Table 2. Benchmarking results of different datasets trained by *PoolNet* [39]. Symbols ↑ and ↓ denote the higher and the lower the better, respectively. Superscript [‡] denotes reported results or results reproduced by public checkpoints.

CoSOD3k [19]	MAE ↓	F_{max} ↑	F_{avg} ↑	E_{max} ↑	E_{avg} ↑	S_{α} ↑
DUTS-TR [‡] [53]	0.1184	0.6961	0.6744	0.7934	0.7707	0.7604
DUTS-Class [66]	0.1132	0.7042	0.6823	0.8011	0.7927	0.7695
Jigsaw [66]	0.1028	0.7243	0.7096	0.8181	0.8059	0.7789
COCO9213 [38]	0.1222	0.7024	0.6719	0.8098	0.7811	0.7621
CAT (Ours)	0.0884	0.7440	0.7313	0.8409	0.8270	0.7914
CAT+ (Ours)	0.0881	0.7448	0.7351	0.8398	0.8303	0.7911

CoCA [66]	MAE ↓	F_{max} ↑	F_{avg} ↑	E_{max} ↑	E_{avg} ↑	S_{α} ↑
DUTS-TR [‡] [53]	0.1822	0.4251	0.4098	0.6751	0.6101	0.6038
DUTS-Class [66]	0.1663	0.4398	0.4270	0.6873	0.6403	0.6200
Jigsaw [66]	0.1644	0.4311	0.4215	0.6684	0.6401	0.6158
COCO9213 [38]	0.1779	0.4301	0.4078	0.6920	0.6351	0.6127
CAT (Ours)	0.1448	0.4399	0.4306	0.6935	0.6767	0.6231
CAT+ (Ours)	0.1447	0.4404	0.4335	0.6909	0.6762	0.6247

Table 3. Benchmarking results of different datasets trained by *EGNet* [67]. Symbols ↑ and ↓ denote the higher and the lower the better, respectively. Superscript [‡] denotes reported results or results reproduced by public checkpoints.

sion and Adam optimizer [31] with learning rate = $4e-5$ and weight decay = $5e-4$. We run this model for 50 epochs. The VGG [48] version of *EGNet* [67] is chosen. We follow the default settings by using the Adam optimizer [31] and assigning the learning rate = $2e-5$, weight decay = $5e-4$, and loss weight = 1. Edge maps are prepared by the corresponding masks of each datasets. We train *EGNet* [67] for 30 epochs and divide the learning rate by 10 after 15 epochs. For *ICNet* [30], we adopt both VGG [48] and ResNet [23] versions of *EGNet* [67] to prepare the single-image-saliency-maps (SISMs). Adam optimizer [31] with learning rate = $8e-6$ is used. We run this model for 80 epochs. For *GICD* [66], we keep the original training paradigm of randomly selecting at most 20 samples from each images groups for each training epoch. Adam optimizer [31] is adopted. The initial learning rate is set as $2e-4$. We train *GICD* [66] for up to 100 epochs and reduce the learning rate to 80% every 20 epochs.

Evaluation. We choose the two recent evaluation datasets *CoSOD3k* [19] and *CoCA* [66] to evaluate model performances. Four conventional metrics are adopted: mean ab-

CoSOD3k [19]	MAE ↓	F_{max} ↑	F_{avg} ↑	E_{max} ↑	E_{avg} ↑	S_α ↑	MAE ↓	F_{max} ↑	F_{avg} ↑	E_{max} ↑	E_{avg} ↑	S_α ↑
DUTS-Class [66]	0.0882	0.7620	0.7537	0.8398	0.8354	0.7976	0.0893	0.7576	0.7499	0.8383	0.8341	0.7933
Jigsaw [66]	0.0887	0.7547	0.7467	0.8357	0.8313	0.7942	0.0967	0.7361	0.7294	0.8150	0.8101	0.7757
COCO9213 [‡] [38]	0.0895	0.7619	0.7517	0.8446	0.8404	0.7936	0.0953	0.7665	0.7431	0.8485	0.8345	0.7966
CAT (Ours)	0.0772	0.7826	0.7687	0.8666	0.8570	0.8104	0.0714	0.7763	0.7681	0.8552	0.8508	0.8092
CAT+ (Ours)	0.0680	0.7907	0.7817	0.8702	0.8656	0.8105	0.0666	0.7919	0.7832	0.8718	0.8670	0.8174
CoCA [66]	MAE ↓	F_{max} ↑	F_{avg} ↑	E_{max} ↑	E_{avg} ↑	S_α ↑	MAE ↓	F_{max} ↑	F_{avg} ↑	E_{max} ↑	E_{avg} ↑	S_α ↑
DUTS-Class [66]	0.1481	0.4728	0.4652	0.7007	0.6673	0.6368	0.1462	0.4694	0.4635	0.7001	0.6766	0.6342
Jigsaw [66]	0.1426	0.4671	0.4609	0.6935	0.6695	0.6372	0.1351	0.4759	0.4701	0.6928	0.6793	0.6412
COCO9213 [38]	0.1470	0.5133	0.5018	0.7042	0.6835	0.6541	0.1546	0.5219	0.4944	0.7166	0.6701	0.6531
CAT (Ours)	0.1126	0.5308	0.5195	0.7497	0.7361	0.6723	0.1011	0.5245	0.5181	0.7396	0.7327	0.6728
CAT+ (Ours)	0.1081	0.5292	0.5218	0.7435	0.7336	0.6729	0.1014	0.5329	0.5256	0.7510	0.7430	0.6783

Table 4. Benchmarking results of different datasets trained by *ICNet* [30]. **Left:** SISMs generated by *EGNet* [67] with VGG [48] backbone; **Right:** SISMs generated by *EGNet* [67] with ResNet [23] backbone. Symbols ↑ and ↓ denote the higher and the lower the better, respectively. Superscript [‡] denotes reported results or results reproduced by public checkpoints.

CoSOD3k [19]	MAE ↓	F_{max} ↑	F_{avg} ↑	E_{max} ↑	E_{avg} ↑	S_α ↑
COCO-SEG [52]	0.0799	0.7673	0.7553	0.8579	0.8526	0.7931
DUTS-Class [66]	0.0815	0.7659	0.7567	0.8493	0.8448	0.8016
Jigsaw [‡] [66]	0.0794	0.7695	0.7628	0.8478	0.8446	0.7969
COCO9213 [38]	0.0837	0.7526	0.7427	0.8427	0.8390	0.7835
CAT (Ours)	0.0727	0.7809	0.7758	0.8602	0.8570	0.8052
CAT+ (Ours)	0.0701	0.7864	0.7785	0.8864	0.8631	0.8121
CoCA [66]	MAE ↓	F_{max} ↑	F_{avg} ↑	E_{max} ↑	E_{avg} ↑	S_α ↑
COCO-SEG [52]	0.1330	0.5082	0.5011	0.7075	0.6955	0.6536
DUTS-Class [66]	0.1502	0.4746	0.4653	0.6735	0.6561	0.6324
Jigsaw [‡] [66]	0.1260	0.5110	0.5043	0.7177	0.7051	0.6563
COCO9213 [38]	0.1431	0.4990	0.4869	0.6985	0.6794	0.6412
CAT (Ours)	0.1187	0.5104	0.5059	0.7230	0.7133	0.6563
CAT+ (Ours)	0.1157	0.5233	0.5159	0.7266	0.7163	0.6676

Table 5. Benchmarking results of different datasets trained by *GICD* [66]. Symbols ↑ and ↓ denote the higher and the lower the better, respectively. Superscript [‡] denotes reported results or results reproduced by public checkpoints.

#	Group	Cut	Paste	MAE ↓	F_{max} ↑	F_{avg} ↑	E_{max} ↑	E_{avg} ↑	S_α ↑
A	◇			.2033	.4187	.4132	.6118	.6015	.5913
B	✓			.1499	.4716	.4661	.6793	.6627	.6331
C	◇		◇	.1783	.4081	.4020	.6305	.6220	.5823
D	◇	✓	◇	.1729	.4166	.4108	.6479	.6348	.5857
E	✓		◇	.1392	.4602	.4559	.6994	.6913	.6268
F	✓	✓	◇	.1302	.4742	.4691	.6999	.6919	.6382
Ours	✓	✓	✓	.1157	.5233	.5159	.7266	.7163	.6676

Table 6. Ablation study for our proposed approach with the *GICD* model on the *CoCA* dataset. Symbols ✓ and ◇ denote conduct and randomly conduct corresponding operations, respectively.

solute error (*MAE*) [8], F-measure [1], E-measure [17], and structure measure (S_α) [16]. For F-measure [1], we follow the convention by setting weight $\beta^2 = 0.3$ and report both the maximum score (F_{max}) and the mean score (F_{avg}). We also report both E_{max} and E_{min} for E-measure [17].

4.2. Quantitative Analysis

Longitudinal Comparison. From Tables 2, 3, 4 & 5, we observe that models trained on CAT/CAT+ achieve better performances than other datasets in all metrics on both *CoSOD3k* [19] and *CoCA* [66]. This suggests that CAT/CAT+ is agnostic to models and backbones. Specifically, the improvements are typically larger in *MAE*. Sig-

nificant boosts for more than 20% are achieved on *PoolNet* [39], *EGNet* [67], and *ICNet* [30], as well as a gain around 10% on *GICD* [66]. Regarding the average improvements on other metrics, we observe that CAT/CAT+ improves more on F-measure ($\sim 9\%$), which shows that instead of radically regarding every foreground objects as salient, models trained on CAT/CAT+ tend to make relatively conservative predictions and focus more on regions with co-salient objects only. This supports our analysis in Sections 1 & 3. It also provides improvements in E-measure ($\sim 7\%$) and S_α ($\sim 3\%$). Indeed, S_α is the hardest among current metrics which measures both accuracy and structural similarity. Although models are capable of making more confident predictions now, they cannot capture very detailed information like boundaries. Overall, we believe that the diversity and quality of CAT/CAT+ have laid the foundation for more in-depth work in the future.

Horizontal Comparison. Changing the direction of comparison, we notice that the evaluation scores on *CoSOD3k* [19] are much higher than *CoCA* [66]. This is in line with the characteristics of these two datasets: although the former is richer in scale, the latter has more complex context and more variant appearance, such as occlusion and object size. Besides, the performances of co-saliency detection models are much better than that of saliency detection models, which emphasize again the importance of specialized modules/techniques designed for identifying co-salient signals and suppressing non-salient ones. In addition, the performance of CAT+ is slightly better than that of CAT. A possible reason for this is that CAT+ has a larger scale, which indeed increases the robustness of the model. We will investigate this potential theory in future work.

Ablation Study. We conduct an ablation study to verify the effectiveness of our methods (see Table 6). The results for the original 8375 images are shown in rows A and B. We also provide other combinations for comparisons, e.g., group images w/ classifiers (vs. randomly allocate images to the same number of groups), cut candidate objects out before paste (vs. do not cut and paste the sampled

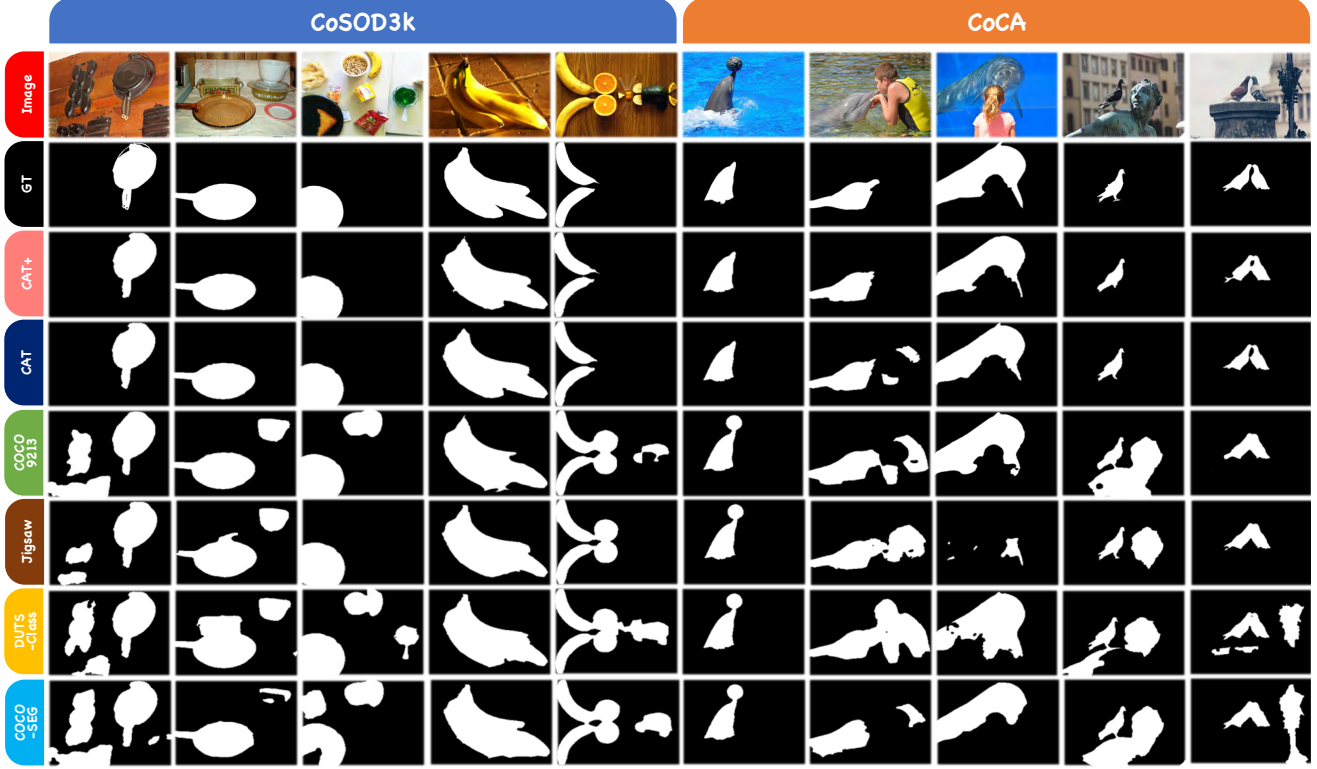


Figure 7. Qualitative results of different datasets trained by *GICD* [66]. **Left:** results on *CoSOD3k* [19]; **Right:** results on *CoCA* [66]. Groups from left to right: *frying pan*, *banana*, *dolphin*, *pigeon*.

images directly), and paste objects/images under counterfactual rules (vs. no paste or randomly paste w/o limitations). Specifically, “*Grouping*” offers proper inter-saliency signals, which is essential for models to find the common salient objects between image groups (A vs. B, C vs. E). “*Cut*” gives fine-grained category information and further improves performance (C vs. D, E vs. F). As the key part, “*Paste*” provides intra-saliency signals, which determines the quality of the collaborative learning paradigm. A proper introduction of such signals significantly boosts the performance (Ours vs. F), and vice versa (A vs. C, B vs. E).

4.3. Qualitative Analysis

Figure 7 illustrates some visualization results on *CoSOD3k* [19] and *CoCA* [66] generated by *GICD* [66] trained with different training datasets. It can be easily observed that the quality of a dataset plays an important role during training. Models encoded with features from high-quality dataset like CAT/CAT+ tends to focus more on the true co-salient signals while suppressing the non-salient ones. Taking the *frying pan* group at columns 1 to 3 as an example. Both semantic segmentation and saliency detection datasets fail to teach the model “what” and “where” to focus and thus let it mistakenly regards items besides *frying pans* as co-salient. In contrast, the model trained

on CAT/CAT+ can well distinguish co-salient objects from non-salient clusters even when they share similar shapes, textures, colors, etc. Please refer to our [supplementary material](#) for more examples. Another point worthy of attention is that the existing models cannot well-restore the details (e.g., the boundaries) of objects, especially that of small objects. For example, the contours of the *pigeons* in the last two columns of Figure 7 are not well drawn. A possible reason for this is that most current co-saliency models adopt VGG-16 [48] as their backbones and rely on low-resolution inputs (e.g., 224×224). Some minor but important features are missing during the down-sampling. With the emergence of more and more deep and efficient backbones, we encourage future works to explore more possibilities.

5. Conclusion

In this work, we addressed the inconsistency problem in co-saliency detection. Borrowing the idea from cause and effect, we proposed a counterfactual training framework to formalize the co-salient signals during training. A group-cut-paste procedure is introduced to leverage existing data samples and makes “cost-free” augmentation by context adjustment. Follow this procedure, we collected a large-scale

dataset call Context Adjustment Training. The abundant semantics and high-quality annotations of our dataset liberates models from the impediment caused by spurious variations and biases and significantly improves model performances. As moving forward, we are going to take a deeper look at the co-salient signals both across image groups and within each sample, and improve the quality and scale of our dataset accordingly.

References

- [1] Radhakrishna Achanta, Sheila Hemami, Francisco Estrada, and Sabine Susstrunk. Frequency-tuned salient region detection. *CVPR*, 2009.
- [2] Dhruv Batra, Adarsh Kowdle, Devi Parikh, Jiebo Luo, and Tsuhan Chen. icoseg: Interactive co-segmentation with intelligent scribble guidance. *CVPR*, 2010.
- [3] Ali Borji, Ming-Ming Cheng, Qibin Hou, Huaizu Jiang, and Jia Li. Salient object detection: A survey. *Comp. Visual Media*, 5(2):117–150, 2019.
- [4] Hwann-Tzong Chen. Preattentive co-saliency detection. *ICIP*, 2010.
- [5] Long Chen, Xin Yan, Jun Xiao, Hanwang Zhang, Shiliang Pu, and Yueting Zhuang. Counterfactual samples synthesizing for robust visual question answering. *CVPR*, 2020.
- [6] Ming-Ming Cheng, Niloy J. Mitra, Xiaolei Huang, and Shi-Min Hu. Salientshape: Group saliency in image collections. *Vis. Comput.*, 30(4):443–453, 2014.
- [7] Ming-Ming Cheng, Niloy J. Mitra, Xiaolei Huang, Philip HS Torr, and Shi-Min Hu. Global contrast based salient region detection. *IEEE Trans. Pattern Anal. Mach. Intell.*, 37(3):569–582, 2014.
- [8] Ming-Ming Cheng, Jonathan Warrell, Wen-Yan Lin, Shuai Zheng, Vibhav Vineet, and Nigel Crook. Efficient salient region detection with soft image abstraction. *ICCV*, 2013.
- [9] Runmin Cong, Jianjun Lei, Huazhu Fu, Qingming Huang, Xiaochun Cao, and Chunping Hou. Co-saliency detection for rgbd images based on multi-constraint feature matching and cross label propagation. *IEEE Trans. Image Process.*, 27(2):568–579, 2017.
- [10] Jifeng Dai, Ying Nian Wu, Jie Zhou, and Song-Chun Zhu. Cosegmentation and cosketch by unsupervised learning. *ICCV*, 2013.
- [11] Jia Deng, Wei Dong, Richard Socher, Li-Jia Li, Kai Li, and Li Fei-Fei. Imagenet: A large-scale hierarchical image database. *CVPR*, 2009.
- [12] Terrance DeVries and Graham W. Taylor. Improved regularization of convolutional neural networks with cutout. *arXiv preprint arXiv:1708.04552*, 2017.
- [13] Santosh K. Divvala, Derek Hoiem, James H. Hays, Alexei A. Efros, and Martial Hebert. An empirical study of context in object detection. *CVPR*, 2009.
- [14] Debidatta Dwibedi, Ishan Misra, and Martial Hebert. Cut, paste and learn: Surprisingly easy synthesis for instance detection. *ICCV*, 2017.
- [15] Deng-Ping Fan, Ming-Ming Cheng, Jiang-Jiang Liu, Shang-Hua Gao, Qibin Hou, and Ali Borji. Salient objects in clutter: Bringing salient object detection to the foreground. *ECCV*, 2018.
- [16] Deng-Ping Fan, Ming-Ming Cheng, Yun Liu, Tao Li, and Ali Borji. Structure-measure: A new way to evaluate foreground maps. *ICCV*, 2017.
- [17] Deng-Ping Fan, Cheng Gong, Yang Cao, Bo Ren, Ming-Ming Cheng, and Ali Borji. Enhanced-alignment measure for binary foreground map evaluation. *IJCAI*, 2018.
- [18] Deng-Ping Fan, Tengteng Li, Zheng Lin, Ge-Peng Ji, Dingwen Zhang, Ming-Ming Cheng, Huazhu Fu, and Jianbing Shen. Re-thinking co-salient object detection. *IEEE Trans. Pattern Anal. Mach. Intell.*, 2021.
- [19] Deng-Ping Fan, Zheng Lin, Ge-Peng Ji, Dingwen Zhang, Huazhu Fu, and Ming-Ming Cheng. Taking a deeper look at co-salient object detection. *CVPR*, 2020.
- [20] Huazhu Fu, Xiaochun Cao, and Zhuowen Tu. Cluster-based co-saliency detection. *IEEE Trans. Image Process.*, 22(10):3766–3778, 2013.
- [21] Shanghua Gao, Ming-Ming Cheng, Kai Zhao, Xin-Yu Zhang, Ming-Hsuan Yang, and Philip HS Torr. Res2net: A new multi-scale backbone architecture. *IEEE Trans. Pattern Anal. Mach. Intell.*, 43(2):652–662, 2021.
- [22] Zhifan Gao, Chenchu Xu, Heye Zhang, Shuo Li, and Victor Hugo C. de Albuquerque. Trustful internet of surveillance things based on deeply represented visual co-saliency detection. *IEEE Internet Things J.*, 7(5):4092–4100, 2020.
- [23] Kaiming He, Xiangyu Zhang, Shaoqing Ren, and Jian Sun. Deep residual learning for image recognition. *CVPR*, 2016.
- [24] Dan Hendrycks, Norman Mu, Ekin D. Cubuk, Barret Zoph, Justin Gilmer, and Balaji Lakshminarayanan. Augmix: A simple data processing method to improve robustness and uncertainty. *ICLR*, 2020.
- [25] Luis Herranz, Shuqiang Jiang, and Xiangyang Li. Scene recognition with cnns: Objects, scales and dataset bias. *CVPR*, 2016.
- [26] David E. Jacobs, Dan B. Goldman, and Eli Shechtman. Cosaliency: Where people look when comparing images. *UIST*, 2010.
- [27] Koteswar Rao Jerripathula, Jianfei Cai, and Junsong Yuan. Cats: Co-saliency activated tracklet selection for video co-localization. *ECCV*, 2016.
- [28] Koteswar Rao Jerripathula, Jianfei Cai, and Junsong Yuan. Efficient video object co-localization with co-saliency activated tracklets. *IEEE Trans. Circuits Syst. Video Technol.*, 2019.
- [29] Huaizu Jiang, Jingdong Wang, Zejian Yuan, Yang Wu, Nan-ning Zheng, and Shipeng Li. Salient object detection: A discriminative regional feature integration approach. *CVPR*, 2013.
- [30] Wen-Da Jin, Jun Xu, Ming-Ming Cheng, Yi Zhang, and Wei Guo. Icnnet: Intra-saliency correlation network for co-saliency detection. *NeurIPS*, 2020.
- [31] Diederik P. Kingma and Jimmy Ba. Adam: A method for stochastic optimization. *ICLR*, 2015.
- [32] Philipp Krähenbühl and Vladlen Koltun. Efficient inference in fully connected crfs with gaussian edge potentials. *NeurIPS*, 2011.

- [33] Yann LeCun, Léon Bottou, Yoshua Bengio, and Patrick Haffner. Gradient-based learning applied to document recognition. *Proc. IEEE*, 1998.
- [34] Bo Li, Zhengxing Sun, Qian Li, Yunjie Wu, and Anqi Hu. Group-wise deep object co-segmentation with co-attention recurrent neural network. *ICCV*, 2019.
- [35] Hongliang Li, Fanman Meng, and King Ng Ngan. Co-salient object detection from multiple images. *IEEE Trans. Multimedia*, 15(8):1896–1909, 2013.
- [36] Hongliang Li and King Ng Ngan. A co-saliency model of image pairs. *IEEE Trans. Image Process.*, 20(12):3365–3375, 2011.
- [37] Tengpeng Li, Kaihua Zhang, Shiwen Shen, Bo Liu, Qingshan Liu, and Zhu Li. Image co-saliency detection and instance co-segmentation using attention graph clustering based graph convolutional network. *IEEE Trans. Multimedia*, 2021.
- [38] Tsung-Yi Lin, Michael Maire, Serge Belongie, James Hays, Pietro Perona, Deva Ramanan, Piotr Dollár, and C. Lawrence Zitnick. Microsoft coco: Common objects in context. *ECCV*, 2014.
- [39] Jiang-Jiang Liu, Qibin Hou, Ming-Ming Cheng, Jiashi Feng, and Jianmin Jiang. A simple pooling-based design for real-time salient object detection. *CVPR*, 2019.
- [40] Zhi Liu, Wenbin Zou, Lina Li, Liquan Shen, and Olivier Le Meur. Co-saliency detection based on hierarchical segmentation. *IEEE Signal Process. Lett.*, 21(1):88–92, 2014.
- [41] Dhruv Mahajan, Ross Girshick, Vignesh Ramanathan, Kaiming He, Manohar Paluri, Yixuan Li, Ashwin Bharambe, and Laurens Van Der Maaten. Exploring the limits of weakly supervised pretraining. *ECCV*, 2018.
- [42] Yulei Niu, Kaihua Tang, Hanwang Zhang, Zhiwu Lu, Xian-Sheng Hua, and Ji-Rong Wen. Counterfactual vqa: A cause-effect look at language bias. *arXiv preprint arXiv:2006.04315*, 2020.
- [43] Judea Pearl. *Causality*. Cambridge University Press, 2009.
- [44] Judea Pearl. Direct and indirect effects. *arXiv preprint arXiv:1301.2300*, 2013.
- [45] Judea Pearl, Madelyn Glymour, and Nicholas P. Jewell. *Causal Inference in Statistics: A Primer*. John Wiley & Sons, 2016.
- [46] Judea Pearl and Dana Mackenzie. *The Book of Why: The New Science of Cause and Effect*. Basic Books, 2018.
- [47] Xiaoliang Qian, Xi Cheng, Gong Cheng, Xiwen Yao, and Liying Jiang. Two-stream encoder gan with progressive training for co-saliency detection. *IEEE Signal Process. Lett.*, 28:180–184, 2021.
- [48] Karen Simonyan and Andrew Zisserman. Very deep convolutional networks for large-scale image recognition. *ICLR*, 2015.
- [49] Satoshi Suzuki. Topological structural analysis of digitized binary images by border following. *Comput. Vis. Graphics Image Process.*, 30(1):32–46, 1985.
- [50] Kaihua Tang, Jianqiang Huang, and Hanwang Zhang. Long-tailed classification by keeping the good and removing the bad momentum causal effect. *NeurIPS*, 2020.
- [51] Antonio Torralba and Alexei A. Efros. Unbiased look at dataset bias. *CVPR*, 2011.
- [52] Chong Wang, Zheng-Jun Zha, Dong Liu, and Hongtao Xie. Robust deep co-saliency detection with group semantic. *AAAI*, 2019.
- [53] Lijun Wang, Huchuan Lu, Yifan Wang, Mengyang Feng, Dong Wang, Baocai Yin, and Xiang Ruan. Learning to detect salient objects with image-level supervision. *CVPR*, 2017.
- [54] Tan Wang, Jianqiang Huang, Hanwang Zhang, and Qianru Sun. Visual commonsense r-cnn. *CVPR*, 2020.
- [55] Wenguan Wang, Qiuxia Lai, Huazhu Fu, Jianbing Shen, Haibin Ling, and Ruigang Yang. Salient object detection in the deep learning era: An in-depth survey. *IEEE Trans. Pattern Anal. Mach. Intell.*, 2021.
- [56] John Winn, Antonio Criminisi, and Thomas Minka. Object categorization by learned universal visual dictionary. *ICCV*, 2005.
- [57] Chuan Yang, Lihe Zhang, Huchuan Lu, Xiang Ruan, and Ming-Hsuan Yang. Saliency detection via graph-based manifold ranking. *CVPR*, 2013.
- [58] Xiwen Yao, Junwei Han, Dingwen Zhang, and Feiping Nie. Revisiting co-saliency detection: A novel approach based on two-stage multi-view spectral rotation co-clustering. *IEEE Trans. Image Process.*, 26(7):3196–3209, 2017.
- [59] Yuanhao Yue, Qin Zou, Hongkai Yu, Qian Wang, and Song Wang. An end-to-end network for co-saliency detection in one single image. *arXiv preprint arXiv:1910.11819*, 2019.
- [60] Zhongqi Yue, Hanwang Zhang, Qianru Sun, and Xian-Sheng Hua. Interventional few-shot learning. *NeurIPS*, 2020.
- [61] Sangdoo Yun, Dongyoon Han, Seong Joon Oh, Sanghyuk Chun, Junsuk Choe, and Youngjoon Yoo. Cutmix: Regularization strategy to train strong classifiers with localizable features. *ICCV*, 2019.
- [62] Dingwen Zhang, Junwei Han, Chao Li, Jingdong Wang, and Xuelong Li. Detection of co-salient objects by looking deep and wide. *Int. J. Comput. Vis.*, 120(2):215–232, 2016.
- [63] Hongyi Zhang, Moustapha Cisse, Yann N. Dauphin, and David Lopez-Paz. mixup: Beyond empirical risk minimization. *ICLR*, 2018.
- [64] Kaihua Zhang, Tengpeng Li, Shiwen Shen, Bo Liu, Jin Chen, and Qingshan Liu. Adaptive graph convolutional network with attention graph clustering for co-saliency detection. *CVPR*, 2020.
- [65] Qijian Zhang, Runmin Cong, Junhui Hou, Chongyi Li, and Yao Zhao. Coadnet: Collaborative aggregation-and-distribution networks for co-salient object detection. *NeurIPS*, 2020.
- [66] Zhao Zhang, Wenda Jin, Jun Xu, and Ming-Ming Cheng. Gradient-induced co-saliency detection. *ECCV*, 2020.
- [67] Jia-Xing Zhao, Jiang-Jiang Liu, Deng-Ping Fan, Yang Cao, Jufeng Yang, and Ming-Ming Cheng. Egnet: Edge guidance network for salient object detection. *ICCV*, 2019.
- [68] Bolei Zhou, Aditya Khosla, Agata Lapedriza, Aude Oliva, and Antonio Torralba. Learning deep features for discriminative localization. *CVPR*, 2016.